

A Database of Underwater Radiated Noise from Small Vessels in the Coastal Area

Shipton, Mark; Obradović, Juraj; Ferreira, Fausto; Mišković, Nikola; Bulat, Tomislav; Cukrov, Neven; Diamant, Roe

Source / Izvornik: **submitted to Scientific Data, 2024**

Journal article, Submitted version

Rad u časopisu, Rukopis poslan na recenzijski postupak (preprint)

Permanent link / Trajna poveznica: <https://um.nsk.hr/um:nbn:hr:168:030404>

Rights / Prava: [In copyright](#)/[Zaštićeno autorskim pravom.](#)

Download date / Datum preuzimanja: **2025-03-14**



Repository / Repozitorij:

[FER Repository - University of Zagreb Faculty of Electrical Engineering and Computing repository](#)



A Database of Underwater Radiated Noise from Small Vessels in the Coastal Area

Mark Shipton^{1,+}, Juraj Obradović^{2,+}, Fausto Ferreira², Nikola Mišković^{2,4}, Tomislav Bulat³, Neven Cukrov³, and Roe Diamant^{1,2,*}

¹University of Haifa, Department of Marine Technology, Haifa, 3498838, Israel

²University of Zagreb, Faculty of Electrical Engineering and Computing, Zagreb, Unska 3, Croatia

³Division for marine and environmental research, Ruder Bošković Institute, Zagreb, 10000, Croatia

⁴CoE MARBLE – Centre of Excellence in Maritime Robotics and Technologies for Sustainable Blue Economy

⁺equal contribution

^{*}Corresponding author: Roe Diamant, roee.d@univ.haifa.ac.il

ABSTRACT

The current procedures for measuring underwater radiated noise (URN) are designed for cooperating vessels in controlled areas. As such, not a lot of data is available for the URN of unidentified vessels of opportunity (VOO), especially for small vessels that do not carry an automatic identification systems (AIS). To this end, we assembled a database of 1148 VOO's URN from acoustic and visual recordings of ferries, fishing boats, yachts, and small speed boats made within Šibenik canal, Croatia. The database comprises source pressure levels at the closest point of approach, picture and video of the vessel, and the vessel's speed, size, and type. A shared webpage allows filtering and comparing vessel types and characteristics. In this paper, we share the structure of our database, the analysis methodology. We conclude that the URN of small vessels is significant and compatible to large vessels.

Background & Summary

Underwater radiated noise (URN) from shipping activity has been identified as a significant component of ocean ambient noise¹⁻³, with recent studies indicating that URN doubles in intensity every decade. The effects of URN on various components of the marine ecosystem, from mussels to marine mammals, have been extensively studied across disciplines⁴. Several reports (e.g.,^{5,6}) suggest that blunt tissue trauma comparable to blast injuries and behavioral changes reflected in social stability and foraging ability have the potential to affect aquatic animals residing in close proximity to a vessel emitting high sound intensities from its propellers or onboard engines. Research has shown that URN from vessel activity leads to a myriad of adverse effects on fish, crustaceans, and especially on cetaceans^{4,7-10}. In particular, the responses of a given aquatic animal to anthropogenic noise can be divided into five main categories¹¹: (I) audibility; (II) behavioral responses reflected in changes in the intensity, frequency and intervals of the animal's vocalizations as well as stress behavior; (III) masking of sounds required for communication, localization and foraging; (IV) physiological auditory threshold shifts due to inner ear hair cell fatigue; and (V) physical damage (injury) to the auditory system. In addition, there are direct risks associated with physical disturbance, as in the cases where sea turtles¹² and large baleen whales¹³ colliding with vessels, partly because the low-frequency sounds from ships interfere with their navigation. Because of these effects, URNs generated by ships are considered a source of pollution and should be monitored regularly by measuring ship noise.

Shipping URN includes high-power impulsive transient waves generated during ignition¹⁴, narrow-band noises generated from thrusters, engines as well pumps and generators¹⁵, and cavitation noises. The latter is caused by the fast enough turn of the propeller to allow low-pressure areas of the propeller to drop below the vapor pressure and the seawater to *boil* at ambient temperature. When the bubbles reach ambient pressure behind the propeller, they implode, yielding broadband stationary noise. The results are: (1) low-frequency noise (around 50 Hz, distributed over a huge area, which impacts the communication of large marine mammals like baleen whales and dolphins); (2) noise from 4-stroke engines (around 200-800 Hz, independent of speed, medium distribution, which likely impacts toothed whales); and (3) high-frequency noise with higher harmonics due to the Lloyd's mirror effect¹⁶ (1 kHz-10 kHz, speed-dependent, which can bear a significant amount of acoustic energy, and likely effects small mammals and fish).

Standards have been established to limit the transmitted acoustic power per exposure time¹⁷, and regulatory organizations such as the European Union, the Convention on the Conservation of Migratory Species (CMS), and the Convention on Biological Diversity (CBD), have adopted resolutions aimed at reducing underwater noise from ships and other man-made noise sources. There have even been recent efforts by the shipping industry to reduce URN by creating special-

41 ized notations for ships that meet certain noise criteria (e.g., <https://www.lr.org/en/knowledge/press-room/press-listing/press-release/lr-announces-new-underwater-noise-notation/>). Although there
42 are standards for quantifying the URN of vessels¹⁸, these require the cooperation of the ship: sailing on a fixed route and at
43 nominal speed. The measurement is carried out at deep sea and under low-noise conditions. These conditions do not apply
44 to the URN measurement of a vessel of opportunity (VOO). Specifically, vessels that are not obliged or avoid carrying an
45 automatic identification system (AIS). As a result, the magnitude of noise from such vessels remains under-explored, and a
46 quantitative study examining the extent of shipping URN has yet to be thoroughly conducted. The main barrier to such studies
47 is the establishment of a proper approach to match the size and type of a vessel to its URN.

48
49 In this paper, we have addressed the challenge of quantifying the URN of VOO by integrating acoustic measurements with
50 video footage processed using machine learning to estimate the vessel's type, speed, and size. This negated the need to detect
51 the vessel's URN in the acoustic data, and the closest point of access (CPA) could be readily analyzed by time synchronization
52 of the optical and acoustic data. The results of our work is an openly shared dictionary for URN of VOO. The data was collected
53 at the entrance to St. Anthony's Channel near Šibenik, Croatia. Through this channel, a daily traffic of hundreds of vessels
54 exists. Most of these vessels do not carry an AIS but are easy to observe visually as they enter or exit the channel. In total, 1148
55 vessels were assessed over a period of 23 days. The measured radiated noise took place right below the vessel, where sound
56 propagation is not affected by seasonal changes. Hence, we argue that the period sampled is representable. Our data comprises
57 pictures and videos of the vessels, the spectrum of their URN at the CPA, and meta-data in the form of the vessel's type, size,
58 height, and speed. In the following, we outline our data collection method, the details of the database and its front-end tool that
59 allows comparison of shipping URN.

60 **Current Approaches in Shipping Noise Measurement**

61 The literature regarding URN measurement focuses on assessing the noise levels and spectral characteristics of various vessel
62 types under different operating conditions (e.g., speed, cargo load, draft, length, and machinery load). There are currently two
63 main approaches for assessing URN from vessels; the first is a "full-control" approach where specific vessels are chartered to
64 conduct measurements under specified operating conditions¹⁹⁻²¹. This approach requires near full control over the measurement
65 and operating conditions (e.g., speed of the vessel, CPA range), thereby enabling highly accurate measurements as well
66 as the ability to conduct repetitive measurements of the same vessel under different operating conditions. However, the
67 cost-effectiveness of this approach also implies that usually, only a small number of vessels is assessed. The second and more
68 prominent approach is the "opportunistic" or *in situ* approach, where sensors and data collecting units are placed near main
69 waterways, and measurements of VOOs are acquired as they transit the area²²⁻²⁴. While the *in situ* approach lacks the ability to
70 control the measurement or operating conditions, it does enable the collection of a larger sample number over longer periods of
71 time.

72 The most common methodology utilized in both the full-control and the *in situ* approaches is cross-referencing acoustic
73 data collected by hydrophones with vessel data. In this aspect, the introduction of the Automatic Identification System
74 (AIS) in the early 2000s has created an accessible and convenient venue for collecting vessel data. The bulk of current
75 research frameworks have primarily depended on AIS for retrieving vessel data^{22,25-27}. While the widespread use of AIS
76 creates more opportunities for full-control and opportunistic URN assessments, it is also important to point out its inherent
77 limitations - as noted in the SOLAS regulation V/19.2 (see <https://www.navcen.uscg.gov/sites/default/files/pdf/AIS/SOLAS.V.19.2.1-5.pdf>), AIS transponders are a legal requirement only for large commercial
78 vessels, e.g., cargo vessels, tankers, passenger ships. This implies that smaller commercial and recreational vessels that are
79 abundant in coastal areas are mostly absent from the current research agenda. The importance of this absence is further
80 emphasized by two aspects. Firstly, the numerical comparison between the number of large commercial vessels and the number
81 of small recreational vessels - the world's total fleet of large commercial vessels is comprised of nearly 109,000 ships (see
82 <https://unctadstat.unctad.org/datacentre/dataviewer/US.MerchantFleet>), while there are nearly
83 12 million recreational vessels in the US alone²⁸. Secondly, the scarce research that has addressed URN from small recreational
84 vessels suggests that under certain conditions, URN from such vessels may be as high or even exceed those of large commercial
85 vessels^{25,29,30}. Accordingly, it would seem imperative that a novel approach for assessing URN from smaller vessels is required
86 to fill this gap.

87
88 The main challenge for conducting wide-scale assessments of small vessels not equipped with AIS is the retrieval of vessel
89 data in order to collect information on the vessel's type, speed, size, and CPA range. This is available through sensors such as
90 radar and HD cameras. Cope et al.²⁹, for example, utilized a multi-sensor system (Marine Monitor - M2) comprised of AIS,
91 Radar, and an HD camera for assessing URN levels of vessels. While this approach enables retrieving essential vessel data such
92 as vessel speed, course, and CPA range, other important parameters, such as vessel size, cannot be accurately assessed. To
93 account for the need to collect acoustic data as well as detailed vessel information accurately, we propose a novel approach
94 based on the integration of acoustic and optical sensors.

95 **Current Approaches in Vessel Detection from Optical Cameras**

96 The methods for detecting ships using cameras are designed to cope with motion and observation noise. The vessel detection
97 approach in³¹ performs background subtraction to detect primary motion in the scene while avoiding interference from wave
98 motion using saliency detection. Similarly, in³², the authors propose a video-based port surveillance that combines context
99 and motion detection. The context part of the algorithm involves graph-based segmentation to identify the ship within the
100 water region, while the motion saliency algorithm utilizes the faster motion of the ship relative to its surroundings. A different
101 approach is proposed in³³, where eigenvalues of region covariance are computed to distinguish man-made objects from the
102 natural background. Another type of scene separation using optical flow is proposed in³⁴ to estimate the moving region in
103 the image, and a Gabor filter is implemented for extracting texture features indicating where the ships are located. However,
104 different possible vessel types make it difficult to achieve robust detection and classification.

105 Due to changing visibility conditions and different shapes of vessels, solutions have recently been developed to identify
106 ships with optical cameras using machine learning methods. These require training with large data sets. For example, the
107 dataset provided in³⁵ contains 5,500 ship images of 109 different classes taken in the Porto Cesareo Marine Protected Area.
108 Results of ship identification using a discriminatively learned CNN are presented. Another dataset is available in³⁶, comprising
109 70,513 vessels, which were recorded in 48,966 images from 10 camera perspectives. As a basis for vessel identification, the
110 authors propose the Single Shot Detector (SSD) algorithm, which supports significant variations in vessel size and aspect ratios.

111 Current approaches to vessel identification are based on transfer learning from already trained models. In³⁷, the YOLOv3-
112 tiny network is used to recognize vessels and distinguish between six vessel types. For the detection of large vessels, which
113 are easily disturbed by surrounding buildings, waves and lights on the water surface, the Convolutional Block Attention
114 Module (CBAM) is used to focus the model on the target vessel. In³⁸, the YOLOv5XL model is used to fuse camera data
115 with AIS information. Through transfer learning, only the last layer was trained with annotated data, which contributes to the
116 generalization of the model. Another application of the YOLOv5 network is presented in³⁹ to classify between vessel types.

117 What distinguishes our work from previous work in vessel detection from optical cameras is the use of the YOLOv5
118 network to detect different types of vessels traveling through narrow canals, and to estimate their size and speed. This system
119 provides more information about the vessel than a bounding box within the image and can manage multiple vessels within a
120 single image. This additional information is used to establish a better link between the vessel's URN and its characteristics and
121 to monitor maritime traffic in narrow areas such as canals, channels, and entrances to marinas with high shipping activity.

122 **Methods**

123 **Visual Analysis**

124 Using shore-fixed camera, we attempt to estimate the size, type and speed of any VOO passing through the Šibenik channel. To
125 this end, we develop a machine learning based model for vessel detection, tracking and classification from video footage. The
126 model provides a bounding box around the vessel. The algorithm then estimates the meter/pixel ratio and determines the size
127 of the boat in meters from the width of the bounding box. In turn, the tracking procedure follows the bounding box through
128 consecutive frames to estimate the vessel's velocity.

129 **Vessel Detection and Classification**

130 For detection, we used the YOLOv5-based trained model which is a fast training model. The details of this implementation are
131 presented in⁴⁰ and are given here in brief for completion. The YOLOv5s model is the second smallest of the YOLOv5 family
132 (see code in <https://github.com/ultralytics/yolov5>). The model includes a backbone based on Darknet53 with
133 Cross Stage Partial (CSP)⁴¹, namely 2 BottleNeckCSP modules and one Spatial Pyramid Pooling (SPP)⁴² block (SPPF) with
134 max pooling (kernel pool size = 5) and a neck based on the Path Aggregation Network (PANet). All convolutional layers used
135 a Sigmoid Linear Unit (SiLU) activation function and batch normalization except the three layers that form the head of the
136 network (Sigmoid function).

137 The model detects and classifies vessels into 9 classes: sailboat, catamaran, small boat, yacht, big yacht, tour boat, passenger
138 boat, trawler, medium boat. For vessel detection and classification, the model was trained using 2100 manually labeled images,
139 observed in 4 different days, and was validated and tested with 100 and 300 images, respectively, captured on days unrelated to
140 the training dataset. Tuned hyper parameters yielded 100 epochs and a batch size of 8. Challenges occur in edge cases when
141 a boat exits the frame, causing the bounding box to start shrinking. Avoiding this, we define a region of interest (ROI) that
142 isolates edge positions.

143 **Vessel Size Estimation**

144 To determine the meter/pixel conversion rates, we used as ground truth 10 vessels from the collected visual data for which the
145 size is known by factory specifications. This small dataset included speedboats, catamarans and tourist boats for which the size
146 can be easily found online. For each boat, up to 3 images were identified showing the vessel in the beginning, middle, and end

Table 1. Boat Dimensions and Pixel Coefficients

Model	Length [m]	Pixel Width	Average Pix. Width	Coefficient	Err to average
Galeon 640 fly	19.81	0.467, 0.467, 0.47, 0.462	0.466	42.438	0.427
Exess 15	14.63	0.366, 0.355	0.361	40.504	2.361
Lagoon 42	12.8	0.295, 0.301, 0.296	0.298	42.940	-0.0745
Antares 650	6.3	0.145, 0.142, 0.144	0.144	43.667	-0.802
Exess 15	14.63	0.359, 0.360, 0.354	0.358	40.827	2.037
Merry F. 1095	10.5	0.248, 0.242	0.245	42.711	0.153
Mali princ	20	0.659, 0.648	0.653	30.585	12.280
Aloha yacht	32.56	0.736	0.736	44.1803	-1.314
Marex 375	12.05	0.280, 0.275, 0.255	0.270	44.549	-1.683
Greenline 40	12.0	0.280, 0.265	0.272	43.969	-1.104
Average coefficient				42.8655	
Standard deviation				1.3485	

147 of the frame. The meter/pixel ratio was calculated for each of the 10 vessels as the relation between real vessel length and
 148 detection bounding box width. A list of all occurrences for the explored 10 vessels is given in Table 1, and examples of the
 149 used frames are given in the Fig. 1.

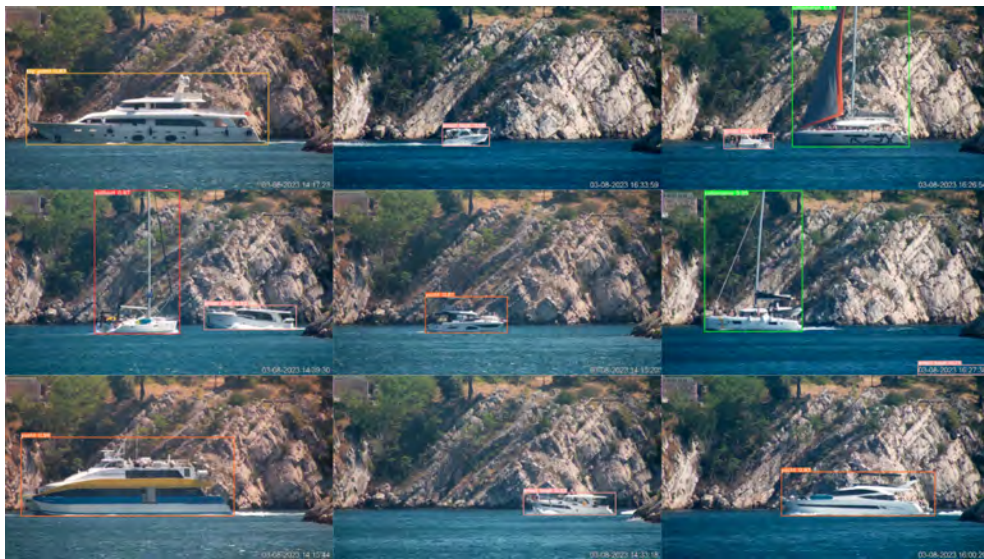


Figure 1. Image detections of the boats used for the estimation of meter/pixel coefficient.

150 **Velocity estimation**

151 For estimating the vessel's speed, we applied the SORT (Simple Online and Realtime Tracking) approach⁴³, which is based on
 152 Kalman filtering. For vessel dynamics, we consider a constant velocity model. We choose SORT due to its ability to maintain
 153 track albeit loos of detection for a few frames. This is a typical scenario in our database due to occlusion events where vessels
 154 cross each other entering or existing the canal. The speed of the vessel is calculated by the distance between the bounding
 155 boxes at consecutive frames, while accounting for the estimated pixel/meter ratio.

156 **Vessel Noise Estimation**

157 **Quality Control**

158 To ensure proper synchronization between the acoustic recorder and HD camera throughout the data collection period, the
 159 system was subjected to a test trial to check for any time drifts. The internal clocks of the acoustic recorder and HD camera
 160 were also compared before and after the data collection period.

161 Acoustic recording of vessel transits were subjected to quality control on three levels: (1) cross-referencing the data with the

162 HD camera, (2) manually reviewing acoustic samples by an expert analyst, and (3) monitoring real-time weather information.
 163 Samples were discarded from the post-analysis under the following criteria.

- 164 1. A vessel transit occurred between recording segments;
- 165 2. Transit occurred in a time frame where wind speed or sea state exceeded ANSI and ISO standards;
- 166 3. If a vessel was employing an active acoustic system (e.g., echo-sounder/Fish-Finder);
- 167 4. If a vessel abruptly changed its course or speed;
- 168 5. If a vessel conducted a north/south transit and did not enter or exit the channel;
- 169 6. If another vessel transited the area within the same time frame;
- 170 7. If a marine fauna noise was detected during the vessel's transit.

171 To calculate the vessel's source level, SL, we reverse-propagate the received acoustic signal, accounting for the transmission
 172 loss, TL, to an idealized monopole @ 1m from the source according to ISO standards⁴⁴, such that

$$SL = SPL + TL . \quad (1)$$

173 This requires the calculation of the SPL and the transmission loss as follows.

174 **Received Noise Levels**

175 Received noise levels (RL) measurements were conducted for the full spectrum of 0.023–24 kHz. The upper-frequency limit is
 176 set by the sampling rate, while the lower limit accounts for the cutoff frequency resulting from the water depth according to
 177 Jensen et al.⁴⁵,

$$f_0 = \frac{c}{4D\sqrt{1 - (c/c_b)^2}}, \quad (2)$$

178 where c is the sound speed in water, c_b is the sound speed in the seabed, and D is the water depth.

179 The time window length used for URN evaluation, which is an essential aspect of the measurement, varies across different
 180 research frameworks. The approach applied in Pine et al.⁴⁶ and Zhang et al.²⁶, for instance, utilized a constant time window
 181 length with no dependence on the length, speed, or range of the vessel. Other approaches chose to apply a variable time window
 182 depending on the vessel's physical characteristics. For example, in Bahtiarian et al.⁴⁷ and McKenna et al.²², the selected time
 183 window was dependent on the time it takes for a vessel to travel its length. Unfortunately, neither of these options is suitable for
 184 our setup. In particular, as the results in Figs. 6, 7 show, our database includes significant variances in vessel transit speeds and
 185 lengths. Instead, we chose to follow the ISO⁴⁴ standard, which sets a variable time window dependent on the aspect of each
 186 vessel (60–120 deg of the bow aspect). Here, the time window length was calculated based on the vessel's speed, as reported by
 187 the visual algorithm.

188 To measure the SPL, we applied (3); the variable time window used for the measurement of each vessel transit was processed
 189 in the frequency domain by a fast-Fourier transform (2048 FFT points, Hanning window with a 50% overlap). The 2048 FFT
 190 resolution was chosen to allow comparability with other research frameworks^{48,49}.

$$SPL = 20\log_{10} \left(\frac{P_{RMS}}{P_{ref}} \right), \quad (3)$$

191 Where $P_{ref} = 1 \mu\text{Pa}$ and P_{RMS} is the root mean square of the sound pressure level measured within the variable time window.
 192 For the measurement of third-octave bands, we applied the same parameters, albeit with a higher frequency resolution (32,768
 193 FFT points), in order to comply with standard one-third octave bands according to the ANSI Standard S1.11-2014/Part 1⁵⁰.

194 **Transmission Loss**

195 The acoustic transmission loss depends on the range of the vessel, geometric spreading characteristics, and the seabed and water
 196 column properties⁵¹. Referring to the vessel's range, while the entrance to the inlet is measured at 135.7 m, our observations
 197 showed that nearly all marine traffic passes through a ~90 m lateral area in the middle of the channel inlet. These observations
 198 coincide with known hazards to safe navigation and official maritime routes described in maritime charts. Based on this
 199 information, we calculate the maximum potential CPA range as the slant between the hydrophone and the described lateral

200 area (49 m) and the minimum potential CPA range as 29 m (water depth to hydrophone). For the geometric transmission loss
201 calculations, we applied the mean CPA range (39 m). This ± 10 m ambiguity in the vessel's location can be compared with the
202 location error of URN databases relying on AIS information, which is known to present a mean discrepancy of up to 97.72 m⁵².

203 In the aspect of absorption losses, applying Ainslie and McColm's⁵³ equation for absorption in seawater for the mean CPA
204 range under different scenarios of temperature and salinity found in the tested area, we reach a maximum loss of roughly 0.15 dB
205 at the mean CPA range. We, therefore, consider absorption losses as negligible. Similar conclusions about the negligibly of
206 absorption losses in URN levels of vessels at close ranges have been made in Hermann et al.⁵⁴ and McKenna et al.²². As the
207 type of sediment in the test bed area consists primarily of fine gravel⁵⁵, which possesses a high reflective coefficient²¹, we
208 chose to apply the simplified equation described by Erbe⁵⁶, which has also been used in similar research frameworks⁵⁷,

$$TL = 20\log_{10}(D) + 10\log_{10}(R/D), \quad (4)$$

209 where R is the horizontal range between the mean CPA and the receiver and we recall that D is the water depth.

210 Data Records

211 The collected data is available in the data repository⁵⁸. In this section we describe the arrangement of the data.

212 Arrangement of Data files

213 Visual Information

214 The optical dataset is organized into 12 folders, each named according to the starting time of the recording in the format
215 yyyyymmdd_hhmmss. Each folder contains pairs of 1-hour video files and corresponding .csv files. In total, there are 324 .csv
216 files. Each .csv file contains detection information with the following columns:

- 217 • `time_of_detection`: The time at which the detection occurred.
- 218 • `boat_class`: The class of the detected boat.
- 219 • `size`: The size of the detected boat.
- 220 • `velocity`: The velocity of the detected boat.

221 An example for the visual data architecture is shown in Fig. 2.

222 Acoustic Information and Online Database

223 The acoustic dataset and processed acoustic information include the time and date of transit, the type of vessel, the sub-type of
224 the vessel, the length and speed of the vessel (according to the visual algorithm), the calculated SL-SPL, and one-third octave
225 spectrogram, and, where applicable, the full name and IMO number.

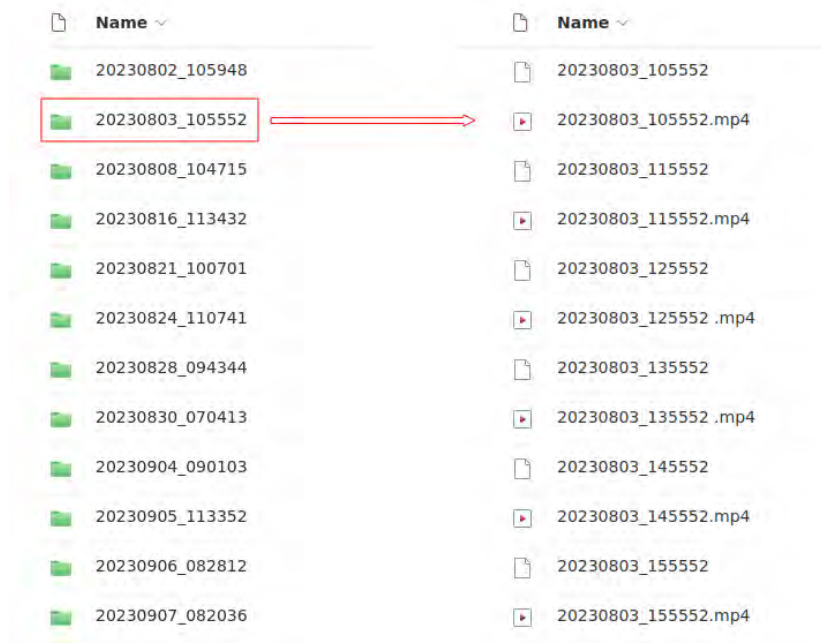


Figure 2. Organisation of the visual data.

226 **Technical Validation**

227 **Description of the Testbed**

228 Our testbed resides in the area of St. Anthony’s Channel (Sv. Ante in local dialect) Inlet near Šibenik, Croatia. During the
 229 summertime, the area is characterized by high-density shipping, which includes various classes of vessels, ranging from coastal
 230 commercial ferries to smaller recreational vessels, e.g., yachts, motorboats, and sailboats. Due to the narrow passage, there is
 231 only one lane within the channel. These conditions make the area an ideal testbed for analyzing underwater radiated noise from
 vessels that are not obligated to carry AIS transponders. An illustration of the testbed is shown in Fig. 3.



Figure 3. Setup of the recorder. Left panel: Illustration of the acoustic-optic testbed for quantifying the URN of VOO by using synchronized optical measurements from a shore based camera and an acoustic recorder positioned at the seabed. Right panel: Picture of the underwater acoustic recorder at the deployment site.

232 On August 2023, an AMAR G3 JASCO acoustic recorder with a single M36-V35-900 Geospectrum omnidirectional
 233

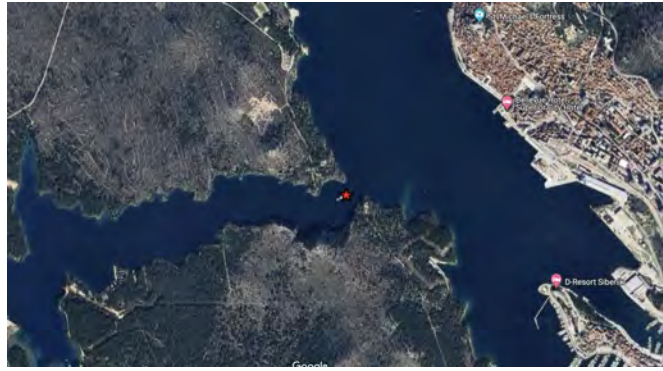


Figure 4. A satellite image of the deployment site. The recorder location is marked in red (right next to the vessel in the image).

234 hydrophone was placed near the eastern entrance to the Channel Inlet at coordinates 43.728400° , 15.879271° (see map in
 235 Fig. 4). The hydrophone had a flat with max 0.5 dB ripple response between 0.01-100 kHz and sensitivity of -164.9 dB
 236 re:1V/ μ Pa. At the point of deployment, the channel is 130.3 m wide and most vessels pass in the middle of the channel. The
 237 recorder was mounted vertically to an anchor one meter above the seabed at a depth of 29 m. The hydrophone's cage was
 238 covered by a dense yellow net to reduce flow noise and assist in locating the recorder after three months of deployment, as
 239 shown in Fig. 3. The recorder was set to record continuously for 12 hours a day between 7:00 to 19:00 (UTC+2) to account for
 240 daylight hours for the specified region at the time of deployment. The recording was made at a sampling rate of 48 kbps, in a
 241 resolution of 3 Bytes per sample. In total, 661 GB were recorded over a period of 113 consecutive days.

242 A DAHUA SD-59230U-HNI (30x optical zoom) video camera was placed roughly 800 m from the entrance to the canal
 243 at coordinates 43.736305° , 15.876754° . The camera was set to continuous recording at a rate of 30 fps with a resolution of
 244 1920×1080 pixels. The camera recorded continuously, however, only recordings during daylight were useful due to the lack of
 245 infra-red recording capability. The video files were stored locally at the camera. In total 340.5 GB were recorded over a period
 246 of 26 days. Example image with two vessels is shown in Fig. 5. For size estimation, the length and height of two landmarks
 were measured. These are the cretaceous limestone layer, both visible in Fig. 5.



Figure 5. Examples of an image with two vessels obtained from the video camera.

247

248 **Vessel Detection Results by Optical Camera**

249 **Summary of Detected Vessels**

250 Our dataset contains 3,799,505 camera detections of various types of vessels, along with their corresponding detection times,
 251 estimated sizes, and velocities. The histogram in Fig. 6 indicates that the "small boat" class is by far the most common in this
 252 dataset, representing around 65% of all detected vessels. Additionally, sailboats are frequently observed, likely due to the
 253 presence of charter marinas in the area. A distribution of vessel sizes is presented in Fig. 7. The data reveals maxima at around
 254 5-8 meters, which is a common size for vessels classified as small boats, and at 12-15 meters, which is typical for regular

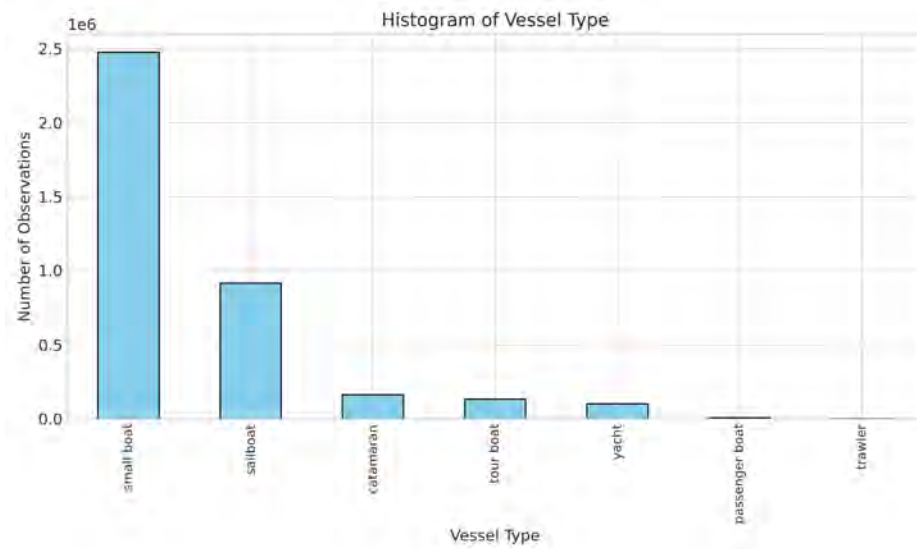


Figure 6. Histogram of vessel classes the final vessel detection result.

sailboats.

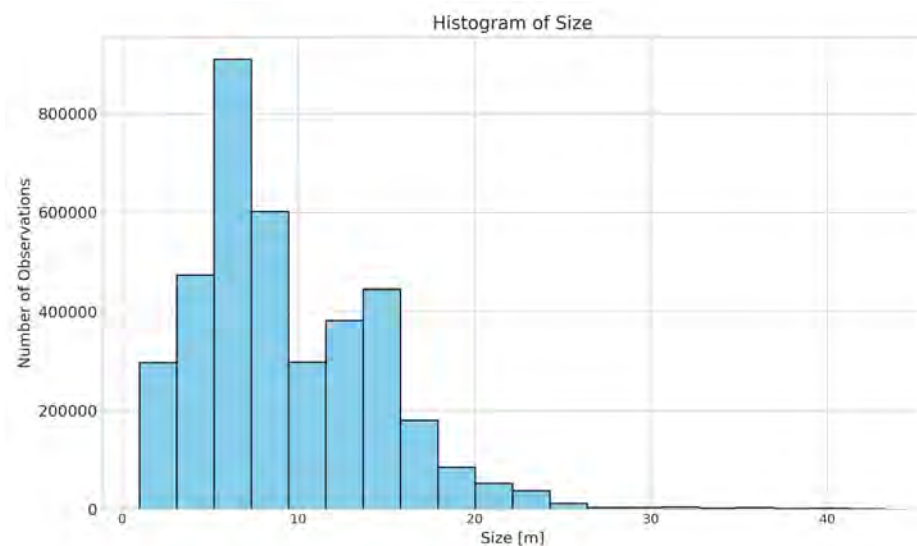


Figure 7. Histogram of vessels size in the final vessel detection result.

255

256

257

258

259

The histogram in Fig. 8 shows the density of vessels' velocities. We determine positive speed for vessels exiting the channel towards the port and vice versa for vessels entering the channel. Results show that vessels moving towards the port move slower compared to those heading towards open sea. Most vessels travel at an absolute speeds of 2.5–4.0 ms⁻¹ (4.85–7.7 knots). This is expected, considering that the most frequently detected class was small boats.

260

Results of Vessel Size and Speed Estimations

261

262

263

264

265

266

To examine the algorithm's performance in estimating vessel size and velocity, a small dataset was created with the vessels of known size and speed. The picture in Fig. 9 is of a small research vessel belonging to the Institute Ruđer Bošković, with a measured waterline length of 8 m and a total length of 9.3 m. To evaluate the size estimation error, the boat performed two transactions on both the left and right sides of the channel. The images collected from 4 such passages are shown in Fig. 9.

Successful detection and classification occur in all frames. However, due to the angle of the vessel, the final part of the stern is included in the bounding box of only some of the frames. Size estimation results of the test vessel for 6 corresponding frames

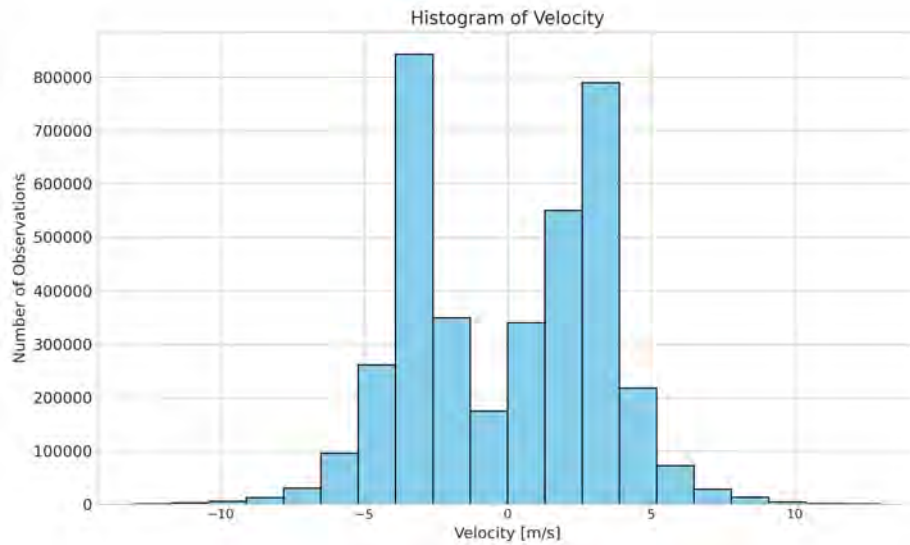


Figure 8. Histogram of vessels velocity in the final vessel detection result. Positive speed reflects vessels exiting the channel, and vice versa for vessels entering the channel.

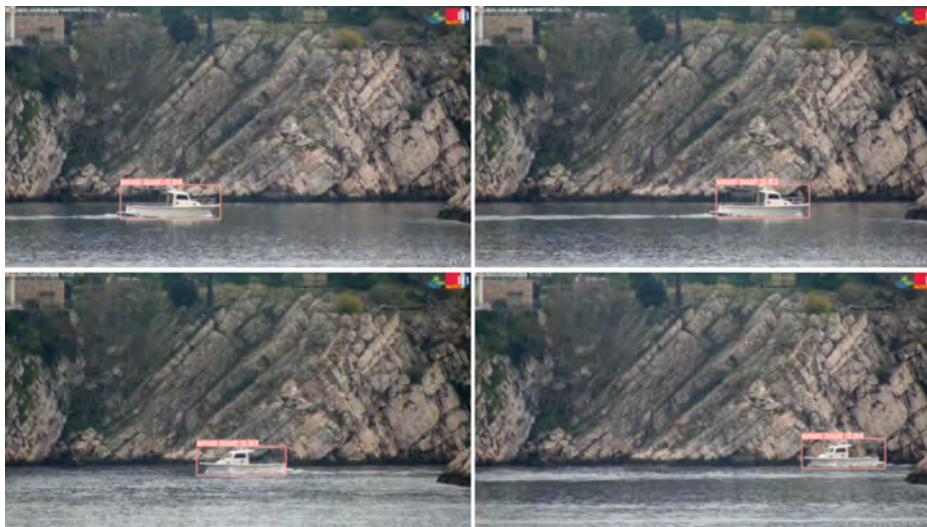


Figure 9. Detections on the vessel with known size for the purpose of algorithm performance evaluation.

267 are given in Table 2. The average length of 8.495 m is close to the waterline length, and a standard deviation of 0.2187 m
 268 represents roughly 3% of the average value. We deem this error acceptable considering the use of a single monocular camera.

269 Another validation of the size and velocity measurements was performed over incidences involving vessels carrying AIS.
 270 To this end, we filtered a large dataset of 65,000 AIS recorded at a low frame rate of 5 min within the channel. That resulted in
 271 only 9 recordings that aligned with the camera frame allowing us to match the AIS data with the camera data accurately. This
 272 low number of vessels emphasizes the low rate of detection available for shipping URN measurements using AIS data only.
 273 The true and estimated size and speed of these 9 vessels are listed in Table 3. An average error of roughly 7% in both length
 274 and speed is observed. Part of this error is due to the rounding operation of the AIS.

275 Results of Shipping Noise Estimation

276 Of the thousands of vessel transits recorded by the visual algorithm, 1148 passed quality control (see Quality Control Section)
 277 and were processed to extract their acoustic characteristics, i.e., sound pressure level and 1/3 octave spectrum. Each vessel
 278 transit was labeled according to its type, the time and date of the transit, as well as the vessel hull name and IMO number, where
 279 applicable. The hull name and IMO no. were associated to a vessel transit in cases where the hull name was visible via the

Table 2. Test results for the Ruđer Bošković Research Vessel (waterline length of 8 m and total length of 9.3 m)

Video Frame	Bounding Box	Estimated Length
1	(0.357, 0.745, 0.214, 0.130)	9.15 m
2	(0.622, 0.743, 0.199, 0.126)	8.53 m
3	(0.794, 0.697, 0.178, 0.113)	7.64 m
4	(0.357, 0.745, 0.214, 0.130)	9.15 m
5	(0.611, 0.727, 0.194, 0.111)	8.33 m
6	(0.508, 0.724, 0.191, 0.111)	8.17 m
Average Length	8.495 m	
Standard Deviation	0.2187 m	

Table 3. Test results for length and speed estimations for 9 vessels identified by both camera and AIS

Boat Index	Length [m]	Estimated Length [m]	Velocity [ms ⁻¹]	Estimated Velocity [ms ⁻¹]
1	12.0	14.48696	6.1	6.99
2	12.0	12.97377	5.1	4.47
3	15.0	16.89319	6.4	6.61
4	15.0	15.37999	5.6	5.25
5	14.0	14.2389	5.0	5.25
6	14.0	14.53657	5.0	5.05
7	17.0	19.39864	6.2	5.44
8	17.0	18.65444	6.4	5.83
9	13.0	13.34587	5.2	5.05
Average error	7.707%		7.395%	
Error Std. Dev	5.368%		4.855%	

280 camera footage. The length and speed of each transit were associated according to the calculations made by the visual algorithm.
 281 Table 4 presents an overview of the analyzed vessels' characteristics, i.e., class, number of observations, speed, length, and the
 282 calculated sound pressure levels at the source (SL-SPL). The largest vessel observed in the dataset was a 54-meter mega-yacht
 283 named "Premier" (IMO 9949132), while the smallest is a 3.3-meter motorboat. The fastest vessel analyzed is a motorboat
 284 sailing at 15.9 meters per second (m/sec), i.e., 31 knots. The slowest vessel is a sailboat sailing at 1.1 m/sec. The loudest vessel
 285 observed was the *Postira* ferry (IMO 6283202) sailing at 6.5 m/sec, which presented a calculated source level of 188.26 dB,
 286 and the quietest vessel was a sailboat sailing at 2.4 m/sec which presented a calculated source level of 151.91 dB.

Table 4. Characteristics of the Vessel Dataset (mean / Std. Dev)

Class	Number of Observations	Speed [m/sec]	Length [m]	SL-SPL [dB]
Ferry	50	5.66 / 0.63	41.95 / 6.43	178.16 / 5.79
Auxiliary Vessel	1	3.5	35.77	176
Cargo Vessel	2	3.1 / 0.28	44	179.45 / 1.916
Fishing Vessel	2	3.60 / 0.28	13.48 / 6.31	167.35 / 0.50
Tour Boat	63	3.44 / 0.61	21.01 / 2.43	167.11 / 4.77
Diving Boat	1	2.80	15.33	172.22
Yacht	124	4.27 / 0.96	25.65 / 10.96	172.12 / 5.64
Sailboat	192	3.22 / 0.63	15.38 / 4.12	162.46 / 5.35
Motor Boat	713	5.15 / 2.00	7.88 / 2.14	170.96 / 4.49
Full Dataset	1148	4.65 / 1.82	13.38 / 9.86	169.79 / 6.12

287 Usage Notes

288 In addition to the dataset file, the data is available at a front end called "Hear my ship" (<https://hearmyship.fer.hr/>).
 289 The web tool allows separation by vessel's type, speed, length and noise, visualization of the data (both optics and acoustics,

290 data download and comparison between the URNs of different vessels.

291 Overall, 1148 vessel transits were evaluated. As mentioned in the introduction Section, URN calculations for small vessels
292 in the coastal area have been mostly absent from the current research agenda, primarily due to the lack of any open-source
293 information systems that broadcast vessel data (e.g., AIS found on larger commercial vessels). This, in turn, creates inherent
294 difficulties in collecting vessel parameters, e.g., length and speed, which are crucial parameters for URN calculations. In this
295 sense, the novel methodology implemented in this research framework enabled the formation of what can be considered the
296 most comprehensive dataset to date, specifically focused on small to medium vessels.

297 In making our database of URN of VOO, our biggest concern was the averaging window around the CPA for URN
298 estimation. The size of this window should be long enough to suppress noise but also short enough to avoid differences in the
299 received power due to the changing distances between the receiver and the moving vessel. In our database, we have followed the
300 method recommended in ISO 17208⁴⁴ that manages this trade-off by setting the observation window as the time-frame in which
301 the vessel passes the $\pm 30^\circ$ aspect tangent to the hydrophone. However, for some of the fast motorboats sailing at >10 m/sec,
302 this resulted in relatively short time-window lengths (~ 4 s). A possible way to address this challenge is a statistical measure to
303 test the stability of the acoustic intensity around the CPA and to determine the size of the observation time accordingly.

304 Another challenge encountered is the extensive traffic of vessels within the channel where the recordings took place. To
305 avoid any mutual interference caused by vessels transiting the channel in close proximity, we placed a strict quality control
306 process (see Section below) and dismissed cases identified by the video footage or acoustics of vessels transiting the channel in
307 close proximity. As a result, roughly 90% of the vessel transits did not pass quality control. The case of too close vessels also
308 poses a challenge for monitoring the URN of VOO in realistic conditions of near port measurements.

309 Code availability

310 The code for the optical and acoustic processing performing ship detection, classification, and size, speed estimation, and
311 acoustic statistical calculations are available in the data repository⁵⁹.

312 References

- 313 1. Wenz, G. M. Acoustic ambient noise in the ocean: Spectra and sources. *The journal acoustical society Am.* **34**, 1936–1956
314 (1962).
- 315 2. Hildebrand, J. A. Anthropogenic and natural sources of ambient noise in the ocean. *Mar. Ecol. Prog. Ser.* **395**, 5–20
316 (2009).
- 317 3. Southall, B. L. *et al.* Underwater noise from large commercial ships—international collaboration for noise reduction.
318 *Encycl. Marit. Offshore Eng.* 1–9 (2017).
- 319 4. Erbe, C. *et al.* The effects of ship noise on marine mammals—a review. *Front. Mar. Sci.* **6**, 476898 (2019).
- 320 5. Gordon, J. *et al.* A review of the effects of seismic surveys on marine mammals. *Mar. Technol. Soc. J.* **37**, 16–34 (2003).
- 321 6. Nelms, S. E., Piniak, W. E., Weir, C. R. & Godley, B. J. Seismic surveys and marine turtles: An underestimated global
322 threat? *Biol. conservation* **193**, 49–65 (2016).
- 323 7. Blom, E.-L. *et al.* Continuous but not intermittent noise has a negative impact on mating success in a marine fish with
324 paternal care. *Sci. reports* **9**, 5494 (2019).
- 325 8. Buscaino, G. *et al.* Impact of an acoustic stimulus on the motility and blood parameters of european sea bass (*dicentrarchus*
326 *labrax* L.) and gilthead sea bream (*sparus aurata* L.). *Mar. environmental research* **69**, 136–142 (2010).
- 327 9. Carter, E. E., Tregenza, T. & Stevens, M. Ship noise inhibits colour change, camouflage, and anti-predator behaviour in
328 shore crabs. *Curr. Biol.* **30**, R211–R212 (2020).
- 329 10. Diamant, R., Testolin, A., Shachar, I., Galili, O. & Scheinin, A. Observational study on the non-linear response of dolphins
330 to the presence of vessels. *Sci. Reports* **14**, 6062 (2024).
- 331 11. Erbe, C., MacGillivray, A. & Williams, R. Mapping cumulative noise from shipping to inform marine spatial planning.
332 *The J. Acoust. Soc. Am.* **132**, EL423–EL428 (2012).
- 333 12. Casale, P. *et al.* Mediterranean sea turtles: current knowledge and priorities for conservation and research. *Endangered*
334 *species research* **36**, 229–267 (2018).
- 335 13. Sèbe, M., Christos, A. K. & Pendleton, L. A decision-making framework to reduce the risk of collisions between ships and
336 whales. *Mar. Policy* **109**, 103697 (2019).
- 337 14. Jensen, F. H. *et al.* Vessel noise effects on delphinid communication. *Mar. Ecol. Prog. Ser.* **395**, 161–175 (2009).

- 338 **15.** Arveson, P. T. & Vendittis, D. J. Radiated noise characteristics of a modern cargo ship. *The J. Acoust. Soc. Am.* **107**,
339 118–129 (2000).
- 340 **16.** Audoly, C. & Meyer, V. Measurement of radiated noise from surface ships-influence of the sea surface reflection coefficient
341 on the lloyd's mirror effect. In *ACOUSTICS 2017* (2017).
- 342 **17.** CMRE. Sonar acoustics handbook by center for maritime research & experimentation (CMRE). In *Animal communication*
343 *and noise*, 20–23 (UComms 18 special edition, 2018).
- 344 **18.** Gassmann, M., Wiggins, S. M. & Hildebrand, J. A. Deep-water measurements of container ship radiated noise signatures
345 and directionality. *The journal acoustical society Am.* **142**, 1563–1574 (2017).
- 346 **19.** Zhu, C., Gaggero, T., Makris, N. C. & Ratilal, P. Underwater sound characteristics of a ship with controllable pitch
347 propeller. *J. Mar. Sci. Eng.* **10**, 328 (2022).
- 348 **20.** Salio, M. P. Numerical assessment of underwater noise radiated by a cruise ship. *Ships Offshore Struct.* **10**, 308–327
349 (2015).
- 350 **21.** Grelowska, G., Kozaczka, E., Kozaczka, S. & Szymczak, W. Underwater noise generated by a small ship in the shallow
351 sea. *Arch. Acoust.* **38**, 351–356 (2013).
- 352 **22.** McKenna, M. F., Ross, D., Wiggins, S. M. & Hildebrand, J. A. Underwater radiated noise from modern commercial ships.
353 *The J. Acoust. Soc. Am.* **131**, 92–103 (2012).
- 354 **23.** Allen, J. K., Peterson, M. L., Sharrard, G. V., Wright, D. L. & Todd, S. K. Radiated noise from commercial ships in the
355 gulf of maine: Implications for whale/vessel collisions. *The J. Acoust. Soc. Am.* **132**, EL229–EL235 (2012).
- 356 **24.** Merchant, N. D., Blondel, P., Dakin, D. T. & Dorocicz, J. Averaging underwater noise levels for environmental assessment
357 of shipping. *The J. Acoust. Soc. Am.* **132**, EL343–EL349 (2012).
- 358 **25.** Veirs, S., Veirs, V. & Wood, J. D. Ship noise extends to frequencies used for echolocation by endangered killer whales.
359 *PeerJ* **4**, e1657 (2016).
- 360 **26.** Zhang, G., Forland, T. N., Johnsen, E., Pedersen, G. & Dong, H. Measurements of underwater noise radiated by commercial
361 ships at a cabled ocean observatory. *Mar. Pollut. Bull.* **153**, 110948 (2020).
- 362 **27.** ZoBell, V. M. *et al.* Underwater noise mitigation in the santa barbara channel through incentive-based vessel speed
363 reduction. *Sci. reports* **11**, 18391 (2021).
- 364 **28.** USCG. 2022 recreational boating statistics (2023). Accessed on 01-07-2024.
- 365 **29.** Cope, S. *et al.* Multi-sensor integration for an assessment of underwater radiated noise from common vessels in san
366 francisco bay. *The J. Acoust. Soc. Am.* **149**, 2451–2464 (2021).
- 367 **30.** Picciulin, M. *et al.* Characterization of the underwater noise produced by recreational and small fishing boats (< 14 m) in
368 the shallow water of the cres-lošinj natura 2000 sci. *Mar. pollution bulletin* **183**, 114050 (2022).
- 369 **31.** Tran, T.-H. & Le, T.-L. Vision based boat detection for maritime surveillance. In *2016 International Conference on*
370 *Electronics, Information, and Communications (ICEIC)*, 1–4 (IEEE, 2016).
- 371 **32.** Bao, X., Zinger, S., Wijnhoven, R. *et al.* Ship detection in port surveillance based on context and motion saliency analysis.
372 In *Video Surveillance and Transportation Imaging Applications*, vol. 8663, 87–94 (SPIE, 2013).
- 373 **33.** Dong, C., Liu, J.-H., Xu, F., Wang, R.-H. *et al.* Fast ship detection in optical remote sensing images. *J. Jilin Univ.*
374 *(Engineering Technol. Ed.)* (2019).
- 375 **34.** Li, H. & Man, Y. Moving ship detection based on visual saliency for video satellite. In *2016 IEEE International Geoscience*
376 *and Remote Sensing Symposium (IGARSS)*, 1248–1250, DOI: [10.1109/IGARSS.2016.7729316](https://doi.org/10.1109/IGARSS.2016.7729316) (2016).
- 377 **35.** Spagnolo, P., Filieri, F., Distanto, C., Mazzeo, P. L. & D'Ambrosio, P. A new annotated dataset for boat detection and
378 re-identification. In *2019 16th IEEE International Conference on Advanced Video and Signal Based Surveillance (AVSS)*,
379 1–7, DOI: [10.1109/AVSS.2019.8909831](https://doi.org/10.1109/AVSS.2019.8909831) (2019).
- 380 **36.** Zwemer, M. H., Wijnhoven, R. G. & de With, P. H. Ship detection in harbour surveillance based on large-scale data and
381 cnns. In *VISIGRAPP (5: VISAPP)*, 153–160 (2018).
- 382 **37.** Li, H., Deng, L., Yang, C., Liu, J. & Gu, Z. Enhanced yolo v3 tiny network for real-time ship detection from visual image.
383 *IEEE Access* **9**, 16692–16706, DOI: [10.1109/ACCESS.2021.3053956](https://doi.org/10.1109/ACCESS.2021.3053956) (2021).
- 384 **38.** Lu, Y. *et al.* Fusion of camera-based vessel detection and AIS for maritime surveillance. In *2021 26th International*
385 *Conference on Automation and Computing (ICAC)*, 1–6 (IEEE, 2021).

- 386 **39.** Gülsoylu, E., Koch, P., Yildiz, M., Constapel, M. & Kelm, A. P. Image and AIS data fusion technique for maritime
387 computer vision applications. In *Proceedings of the IEEE/CVF Winter Conference on Applications of Computer Vision*,
388 859–868 (2024).
- 389 **40.** Correia, A., Ferreira, F. & Mišković, N. Comparing different yolo versions for boat detection and classification in real
390 datasets. In *OCEANS 2024 Singapore* (IEEE, 2024). Accepted for publication.
- 391 **41.** Wang, C.-Y. *et al.* Cspnet: A new backbone that can enhance learning capability of cnn. In *2020 IEEE/CVF Conference on*
392 *Computer Vision and Pattern Recognition Workshops (CVPRW)*, 1571–1580, DOI: [10.1109/CVPRW50498.2020.00203](https://doi.org/10.1109/CVPRW50498.2020.00203)
393 (2020).
- 394 **42.** He, K., Zhang, X., Ren, S. & Sun, J. Spatial pyramid pooling in deep convolutional networks for visual recognition. *IEEE*
395 *Transactions on Pattern Analysis Mach. Intell.* **37**, 1904–1916, DOI: [10.1109/TPAMI.2015.2389824](https://doi.org/10.1109/TPAMI.2015.2389824) (2015).
- 396 **43.** Bewley, A., Ge, Z., Ott, L., Ramos, F. & Upcroft, B. Simple online and realtime tracking. In *2016 IEEE international*
397 *conference on image processing (ICIP)*, 3464–3468 (IEEE, 2016).
- 398 **44.** for Standardization, I. O. Iso/dis 17208-3(en) underwater acoustics — quantities and procedures for description and
399 measurement of underwater sound from ships — part 3: Requirements for measurements in shallow water (2019).
400 [Accessed 10-06-2024].
- 401 **45.** Jensen, F. B., Kuperman, W. A., Porter, M. B., Schmidt, H. & Tolstoy, A. *Computational ocean acoustics*, vol. 2011
402 (Springer, 2011).
- 403 **46.** Pine, M. K., Jeffs, A. G., Wang, D. & Radford, C. A. The potential for vessel noise to mask biologically important sounds
404 within ecologically significant embayments. *Ocean. & Coast. Manag.* **127**, 63–73 (2016).
- 405 **47.** Bahtiarian, M. A. Asa standard goes underwater. *Acoust. Today* **5**, 26–29 (2009).
- 406 **48.** Mahanty, M. M., Latha, G., Raguraman, G., Venkatesan, R. *et al.* Passive acoustic detection of distant ship crossing signal
407 in deep waters using wavelet denoising technique. In *OCEANS 2022-Chennai*, 1–5 (IEEE, 2022).
- 408 **49.** Song, G. *et al.* Underwater noise classification based on support vector machine. In *2021 OES China Ocean Acoustics*
409 *(COA)*, 410–414 (IEEE, 2021).
- 410 **50.** ANSI. ANSI/ASA S1.11-2014/Part 1 / IEC 61260:1-2014 - Electroacoustics - Octave-band and Fractional-octave-band
411 Filters - Part 1: Specifications (a nationally adopted international standard — webstore.ansi.org (2014). [Accessed
412 10-06-2024].
- 413 **51.** Marsh, H. & Schulkin, M. *Underwater sound transmission* (Avco Corporation, Marine Electronics Office, 1962).
- 414 **52.** Jankowski, D., Lamm, A. & Hahn, A. Determination of ais position accuracy and evaluation of reconstruction methods for
415 maritime observation data. *IFAC-PapersOnLine* **54**, 97–104 (2021).
- 416 **53.** Ainslie, M. A. & McColm, J. G. A simplified formula for viscous and chemical absorption in sea water. *The J. Acoust. Soc.*
417 *Am.* **103**, 1671–1672 (1998).
- 418 **54.** Hermannsen, L., Beedholm, K., Tougaard, J. & Madsen, P. T. High frequency components of ship noise in shallow water
419 with a discussion of implications for harbor porpoises (*phocoena phocoena*). *The J. Acoust. Soc. Am.* **136**, 1640–1653
420 (2014).
- 421 **55.** Huljek, L., Strmić Palinkaš, S., Fiket, Ž. & Fajković, H. Environmental aspects of historical ferromanganese tailings in the
422 šibenik bay, croatia. *Water* **13**, 3123 (2021).
- 423 **56.** Erbe, C. Underwater acoustics: noise and the effects on marine mammals. *A Pocket Handb.* **164**, 10–35 (2011).
- 424 **57.** Sipilä, T., Viitanen, V., Uosukainen, S. & Klose, R. Shallow water effects on ship underwater noise measurements. In
425 *48th International Congress and Exhibition on Noise Control Engineering, INTER-NOISE 2019*, 1707 (Institute of Noise
426 Control Engineering, 2019).
- 427 **58.** Obradović, J. & Shipton, M. Raw data for the hearmyship data repository: optical and acoustic files of vessels, DOI:
428 [10.57760/sciencedb.13099](https://doi.org/10.57760/sciencedb.13099) (2024). [Accessed 11-09-2024].
- 429 **59.** Obradović, J. & Shipton, M. Code for the processing of the hearmyship data repository: optical and acoustic, DOI:
430 <https://doi.org/10.57760/sciencedb.13532> (2024). [Accessed 11-09-2024].

431 **Acknowledgements**

432 The authors would like to thank Shlomi Dahan and Mak Gračić for their help in acquiring the acoustic data, and to Matej
433 Radović and Đula Nađ for their help in setting up the web front.

434 This research was supported by a scholarship sponsored by the Israeli Science Foundation (grant #973/23), by the University
435 of Haifa's Innovation & Sustainability Division, and by the Horizon Europe program of the European Union under the
436 UWIN-LABUST project (project #101086340).

437 **Author contributions statement**

438 MS analyzed the acoustic data, created the database, and wrote the manuscript; JO and FF analyzed the visual data and wrote
439 the manuscript; NM assisted with administration, provided funding, and edited the manuscript; TB and NB acquired the
440 acoustic and visual data; RD supervised the project, acquired the acoustic dataset, provided funding and wrote the manuscript.

441 **Competing interests**

442 The author(s) declare no competing interests.